# Mid-upper tropospheric methane in the high Northern Hemisphere: Spaceborne observations by AIRS, aircraft measurements, and model simulations

Xiaozhen Xiong,[1,2] Christopher D. Barnet,[2] Qianlai Zhuang,[3] Toshinobu Machida,[4] Colm Sweeney,[5] and Prabir K. Patra[6]

Received 31 December 2009; revised 29 June 2010; accepted 6 July 2010; published 9 October 2010.

[1] Spaceborne measurements by the Atmospheric Infrared Sounder (AIRS) on the EOS/Aqua satellite provide a global view of the methane ($CH_4$) distribution in the mid-upper troposphere (MUT-$CH_4$). The focus of this study is to examine the spatiotemporal variation of MUT-$CH_4$ in the high Northern Hemisphere (HNH) using AIRS retrievals, aircraft measurements, and simulations from a forward chemistry-transport model (i.e., ACTM). Data from 2004 and 2005 focusing over two regions (Alaska and Siberia) are analyzed. An important feature in the seasonal variation of $CH_4$ we found is the summer increase of MUT-$CH_4$, which is nearly opposite to the summer minimum of $CH_4$ in the marine boundary layer (MBL). This study also demonstrated an apparent increase of $CH_4$ over Alaska associated with the 2004 Alaska forest fire and a negative bias of the ACTM simulations in the HNH. The larger bias of the model simulations in the late winter to early spring may indicate possible unidentified $CH_4$ emission sources (e.g., the use of energy or gas leakage) during this period, but more studies will be needed due to the retrieval uncertainties in the polar winter season. The summer increase of MUT-$CH_4$ is related to surface emission, but the enhanced convection in summer is likely the most important driver.

**Citation:** Xiong, X., C. D. Barnet, Q. Zhuang, T. Machida, C. Sweeney, and P. K. Patra (2010), Mid-upper tropospheric methane in the high Northern Hemisphere: Spaceborne observations by AIRS, aircraft measurements, and model simulations, *J. Geophys. Res.*, *115*, D19309, doi:10.1029/2009JD013796.

## 1. Introduction

[2] As one of the most important greenhouse gases, atmospheric methane ($CH_4$) is 25 times more effective on a per unit mass basis than carbon dioxide in absorbing long-wave radiation on a 100 year time horizon, and accounts for 18% of the total of 2.66 W $m^{-2}$ of the anthropogenically produced greenhouse gas radiative forcing [*Intergovernmental Panel on Climate Change*, 2007]. It also plays an important role in atmospheric ozone chemistry (e.g., in the presence of nitrogen oxides, tropospheric methane oxidation will lead to the formation of ozone), and increase in water vapor in the stratosphere [*Brasseur et al.*, 1999]. The concentration of $CH_4$ over the globe has risen dramatically since the preindustrial era [*Rasmussen and Khalil*, 1984; *Nakazawa et al.*, 1993; *Dlugokencky et al.*, 1995]. However, the observed rate of increase varies significantly. For example, an anomalous large increase of the growth rate of $CH_4$ was observed in 1998, but this was followed by a period of very little to no increase since 2000 [*Dlugokencky et al.*, 2003; *Simpson et al.*, 2002] until a renewed increase was found in 2007 and 2008 [*Rigby et al.*, 2008; *Dlugokencky et al.*, 2009]. The anomalous increase of the growth rate of $CH_4$ in 1998 was partially attributed to wetland emission [*Dlugokencky et al.*, 2001], and/or anomalously high biomass burning [*Butler et al.*, 2005]. The increase of $CH_4$ in 2007 was largely caused by wetlands with a large tropical contribution [*Rigby et al.*, 2008], and *Dlugokencky et al.* [2009] suggested the most likely drivers of the $CH_4$ anomalies during 2007 and 2008 were greater than average precipitation in the tropics plus anomalously high temperatures in the Arctic. Recent studies show that the flattening of the growth rate since 2000 is caused by the fairly constant anthropogenic emission of $CH_4$ [*Dlugokencky et al.*, 2003; *Patra et al.*, 2009a], and a large part of the interannual variability in $CH_4$ growth rate in the tropical latitudes can be explained by the variations in atmospheric transport [*Patra et al.*, 2009a], variations in wetland emissions [*Bousquet et al.*, 2006] and small changes in sinks [e.g., *Wang et al.*, 2004; *Fiore et al.*, 2006].

[3] Quantification of methane emissions still has large uncertainties mainly due to the undersampling of $CH_4$ concentrations over most regions of the globe by the surface

[1]Dell Perot Systems Government Services, Fairfax, Virginia, USA.
[2]Center for Satellite Applications and Research, National Environmental Satellite, Data, and Information Service, NOAA, Camp Springs, Maryland, USA.
[3]Department of Earth and Atmospheric Sciences and Department of Agronomy, Purdue University, West Lafayette, Indiana, USA.
[4]CGER, National Institute for Environmental Studies, Tsukuba, Japan.
[5]Global Monitoring Division, ESRL, NOAA, Boulder, Colorado, USA.
[6]Research Institute for Global Change, JAMSTEC, Yokohama, Japan.


0148-0227/10/2009JD013796

observation network, and one of the large uncertainties is the emission from the high northern latitude regions, particularly the release of $CH_4$ from the thawing permafrost [*Zhuang et al.*, 2009]. The carbon-rich arctic soils and lakes are underlain with either continuous or discontinuous permafrost, thereby constituting a large reservoir of carbon that contains an estimated 700–950 Pg-C in the top 1–25 m [*Zimov et al.*, 2006]. Currently, $CH_4$ is released from both thawing lakes and soils [*Walter et al.*, 2006]. *Shakhova et al.* [2010] recently reported convincing evidence of $CH_4$ outgassing from the Arctic continental shelf off northeastern Siberia (Laptev and East Siberia Sea), and the estimated annual outgassing to the atmosphere is ~8 Tg C. An increase in permafrost degradation and the shoreline erosion of existing lakes, along with the formation of new permafrost-thawing lakes, are expected due to continued climate warming, and these changes could increase $CH_4$ emissions from these lakes by several orders of magnitude [*Walter et al.*, 2007]. The thawing of subarctic peatland permafrost was observed to accelerate over the last 50 years in the discontinuous permafrost zone of northern Canada (53°N–58°N) [*Payette et al.*, 2004]. Field measurements showed that $CH_4$ emission from mires increased by about 22–66% over the period of 1970 to 2000 and this increase is associated with the permafrost and vegetation changes [*Christensen et al.*, 2004]. *Bloom et al.* [2010] estimated that $CH_4$ emissions from temperate Northern Hemisphere latitude wetlands rose by ~6 Tg C per year between 2003 and 2007.

[4] Current ground-based measurements of $CH_4$ are spatially sparse and not representative at large scales in the subarctic wetlands and permafrost regions [see *GLOBALVIEW-CH4*, 2009]. Comparisons of model results and limited ground-based measurements indicate that models have difficulty in reproducing seasonal cycles at higher latitude stations of the Northern Hemisphere because of the local emissions [*Houweling et al.*, 2000; *Wang et al.*, 2004], although the model results are sensitive to the parameterization of wetland emission [*Houweling et al.*, 2000]. Some improvements have been achieved recently by choosing a particular combination of sources [*Patra et al.*, 2009a, and references therein].

[5] Reaction with OH constitutes the main sink for $CH_4$, and the complexity in estimating the wetland emission and the increase of OH in the summertime, along with the uncertainty in the simulation of transport by model, makes the $CH_4$ simulations difficult in the high Northern Hemisphere (HNH). There is even less knowledge of the vertical variation of the $CH_4$ in the HNH due to the lack of measurements. To our knowledge, multiple years' in situ profile observations in the HNH include only aircraft measurements near Poker Flat, Alaska (65°N, 147°W) since 1999 [*GLOBALVIEW-CH4*, 2009], and near Surgut, Siberia (61°N, 73°W) since the early 1990s [*Machida et al.*, 2001; *Barkley et al.*, 2007], but both of which were made, in general, at an interval of once or twice in a month. The most recent aircraft measurements devoted to the HNH were carried out in the campaign of Arctic Research of the Composition of the Troposphere from Aircraft and Satellite (ARCTAS) in the spring and summer of 2008 (http://www-air.larc.nasa.gov/missions/arctas/arctas.html) [*Jacob et al.*, 2010].

[6] In recent years, spaceborne remote sensing has been employed for the measurement of $CH_4$ with large spatial and temporal coverage. Two popular techniques are the measurements of the mid-upper tropospheric $CH_4$ using the thermal infrared (IR) spectrum and the measurements of the total column using the near-IR spectrum. $CH_4$ profile observations from space using the thermal IR spectrum include the Interferometric Monitor for Greenhouse Gases (IMG) onboard the Advanced Earth Observing Satellite (ADEOS) [*Clerbaux et al.*, 2003], the Tropospheric Emission Spectrometer (*TES*) on NASA/Aura [*Payne et al.*, 2009], the AIRS on NASA/AQUA [*Aumann et al.*, 2003], and the Infrared Atmospheric Sounding Interferometer (*IASI*) on METEOP-1 [*Crevoisier et al.*, 2009; *Razavi et al.*, 2009]. $CH_4$ total column observations using near-IR spectrum include the SCanning Imaging Absorption spectroMeter for Atmospheric CartograpHY (SCIAMACHY) instrument onboard ENVISAT [*Frankenberg et al.*, 2008]. The most recent mission is the Greenhouse gases Observation SATellite (GOSAT), which carries the Thermal And Near-infrared Sensor for carbon Observation (TANSO) [*Yokota et al.*, 2008]. These satellite observations have provided another observational window into the natural methane cycle [*Heimann*, 2010], which, for example, enabled better understanding of the emissions and transport near the tropics [*Frankenberg et al.*, 2008; *Crevoisier et al.*, 2009] and over south Asia [*Xiong et al.*, 2009a]. However, space observations of $CH_4$ are more challenging in the HNH using either the thermal IR or near-IR sensors, since the near-IR measurements rely on the absorption spectra of solar radiation and its sensitivity decreases for large solar zenith angles, and the sensitivity of thermal IR measurements to gas absorption becomes smaller for colder temperature and lower vertical temperature contrasts (i.e., lower temperature lapse rates).

[7] This paper presents an approach to understanding the spatiotemporal variations of mid-upper tropospheric $CH_4$ in the HNH (with latitudes >45°N), particularly over Alaska-Canada and Siberia where the wetlands and permafrost mostly underlie, using the AIRS retrieved $CH_4$. The advantage to use thermal IR (i.e., AIRS) rather than near-IR instrument is its capability to measure the $CH_4$ profile [*Xiong et al.*, 2008a], thus providing some information of the $CH_4$ distribution in the mid-upper troposphere. A description to the AIRS retrieval of $CH_4$ and the derivation of MUT-$CH_4$ is given in section 2. In situ aircraft measurements, model simulations from ACTM [*Patra et al.*, 2009b] and the method to use the AIRS averaging kernels to convolve the model data are also introduced in section 2. Section 3 discusses some features of the spatiotemporal variation of mid-upper tropospheric $CH_4$ over Alaska-Canada and Siberia based on the AIRS derived MUT-$CH_4$ and aircraft measurements. A detailed comparison of AIRS $CH_4$ with model simulations, which are sampled at the same time intervals as AIRS observations and convolved using averaging kernels, is also presented. Some discussion of the possible factors impacting the seasonal cycles, particularly the enhanced wetland emission and convection during summer, is given in section 4.

## 2. Data and Methods

### 2.1. AIRS Measurement of $CH_4$

[8] AIRS was launched in polar orbit (13:30 local time, ascending node) on the EOS/Aqua satellite in May 2002. It has 2378 channels covering 649–1136, 1217–1613 and

2169–2674 $cm^{-1}$ at high spectral resolution ($\lambda/\Delta\lambda = 1200$) [*Aumann et al.*, 2003], and the noise, which is represented as the equivalent change in temperature ($Ne\Delta T$) at a reference temperature of 250 K, ranges from 0.14 K in the 4.2 $\mu$m lower tropospheric sounding wavelengths to 0.35 K in the 15 $\mu$m upper tropospheric sounding region. The spatial resolution of AIRS is 13.5 km at nadir, and in a 24 h period AIRS normally observes the complete globe twice per day. In order to retrieve $CH_4$ in both clear and partial cloudy scenes, 9 AIRS fields of view (FOVs) within the footprint of the Advanced Microwave Sounding Unit (AMSU) are used to derive a single cloud-cleared radiance spectrum in what is called a field of regard (FOR), The cloud-cleared FOR radiance spectrum is then used for retrieving profiles with a spatial resolution of about 45 km. There are 71 AIRS channels near 7.6 $\mu$m and a series of seven vertically overlapping trapezoidal functions: 0.016–32 hPa, 32–160 hPa, 160–260 hPa, 260–359 hPa, 359–460 hPa, 460–596 hPa, and 596–1100 hPa that are used for $CH_4$ retrieval. The $CH_4$ first guess profile ("a priori") in the retrieval is given as a function of latitude and pressure (to capture its strong latitudinal and vertical gradients), and is generated by using a nonlinear polynomial fitting to some in situ aircraft measurements and model data [see *Xiong et al.*, 2008a]. The atmospheric temperature profile, water profile, surface temperature and surface emissivity required as inputs in $CH_4$ retrieval are derived from other AIRS channels using the version 5 of AIRS product retrieval software. These data are available at the NASA Goddard Earth Sciences Data and Information Services Center (DISC) (http://disc.gsfc.nasa.gov/AIRS/index.shtml/). An "offline" version of the AIRS product is run at NOAA National Environmental Satellite, Data, and Information Service (NESDIS), Center for Satellite Application and Research (STAR), where the data are thinned to a 3° × 3° spatial grid, and these data are available at NOAA/NESDIS/STAR by request. Two years of 3° × 3° data (2004 and 2005) are analyzed in this paper.

[9] One challenge in analyzing products from thermal IR sounders, such as AIRS, is the change of information content of the retrievals in time and space. For example, information content, and the layers where sensitivity is greatest, depend on atmospheric and surface state variables (temperature and moisture profiles, as well as surface temperature and emissivity) [*Xiong et al.*, 2008a; *Crevoisier et al.*, 2009; *Payne et al.*, 2009; *Razavi et al.*, 2009]. Thus interpretation of $CH_4$ variations based on the retrieved values alone might be misleading if the change of information content of the retrievals, as well as the a priori information used in the retrieval, are not taken into account. An appropriate comparison of the $CH_4$ seasonal cycle from AIRS retrievals with that from either the model simulations or in situ aircraft measurements thus, strictly speaking, needs to utilize the averaging kernels [*Xiong et al.*, 2008a]. However, analysis of satellite retrieved $CH_4$ without averaging kernels is useful for studying the $CH_4$ variation in regions lacking in situ observations. The approach of using the retrieved $CH_4$ in a fixed geographical layer for analysis is appropriate to illustrate the spatiotemporal variation approximately in the mid-low latitude regions, but this is not recommended in the HNH due to the large seasonal variation of the maximum sensitive layer. One way, as suggested by *Xiong et al.* [2009b], is to use the retrieved $CH_4$ around the maximum sensitive layer of AIRS (i.e., the layer 50 to 250 hPa below the tropopause) for analyzing the mid-upper tropospheric $CH_4$. For simplification, in this work the AIRS $CH_4$ at the layer 50 to 250 hPa below the tropopause is designated as "MUT-$CH_4$," which is derived on basis of the retrieved $CH_4$ mixing ratio in 100 levels and the tropopause height. The tropopause height is computed using the corresponding temperature profile retrieved from AIRS. For a typical tropopause height around 250 hPa in summer in the HNH, MUT-$CH_4$ represents the mean $CH_4$ mixing ratio in a thick layer around 300–500 hPa, which covers 13 layers of the 100 layers grid in the AIRS forward model.

[10] The dominant uncertainties in AIRS retrievals arise from (1) the errors in radiative transfer computation, including the input atmospheric temperature and moisture profiles, surface temperature and emissivity, (2) the errors in cloud/clearing, and (3) the noise of the sensor. Since the ground surface is mostly covered by snow/ice and the thermal contrast in the troposphere is small in the arctic winter, the errors in the retrieved temperature, water vapor, and surface temperature and emissivity could be relatively larger than in other seasons, thus lead to a larger uncertainty in $CH_4$ retrieval. An upper estimate of the effect of instrument noise was calculated by assuming a noise equivalent bias in radiance, which resulted in a $CH_4$ retrieval bias of 26 ppbv at 200–400 hPa and less than 10 ppbv below 500 hPa (with the standard deviation of less than 10 ppb) [see *Xiong et al.*, 2008a]. However, this random error from noise can be reduced significantly by averaging the retrievals within a large area with a radius of a few hundred kilometers. The $CH_4$ retrieval errors resulting from the input temperature and moisture profile can be estimated from the change of retrieved $CH_4$ after including the temperature and moisture profile biases in the AIRS products. As demonstrated by *Xiong et al.* [2008a], these errors are within the noise equivalent bias/error. Errors in cloud-clearing impact all the retrieval products from AIRS, so it is difficult to isolate its impact on the $CH_4$ retrievals. However, an analysis of the relation between the AIRS retrieved $CH_4$ in an area within a radius of 200 km with cloud amount indicated that the difference of $CH_4$ between clear cases (with the cloud fraction less than 0.1) and cloud cases (with the cloud fraction over 0.8) is usually less than 1.0%, and no systematic bias associated with cloud amount has been found. Validation using in situ aircraft observations mostly over North America, operated by NOAA/ESRL/GMD, from 2003 to 2006 showed that the bias of the retrieved $CH_4$ profiles is approximately −1.4∼+0.1% and its root mean square (RMS) difference is about 0.5–1.6% [*Xiong et al.*, 2008a]. Validation of MUT-$CH_4$ using aircraft measurements from NOAA/ESRL/GMD and the NASA campaigns Intercontinental Chemical Transport Experiment (INTEX) INTEX-A and INTEX-B demonstrated that in the HNH the RMS error of AIRS MUT-$CH_4$ is less than 1.2%, and the correlation coefficient between AIRS MUT-$CH_4$ and the aircraft measurements is about 0.6–0.7 [*Xiong et al.*, 2009b]. Note in the AIRS version 5 we added a 2% bias correction to the absorption coefficients for strong $CH_4$ absorption channels near 1306 micron. This may result in a negative bias in the retrievals, and will be the subject of future research.

### 2.2. Aircraft Measurements

[11] Aircraft measurements of $CH_4$ used later in this paper include the measurements over Poker Flat, Alaska (PFA),

and Surgut, Siberia. Aircraft measurements over PFA are operated by the NOAA Earth System Research Laboratory, Global Monitoring Division (NOAA/ESRL/GMD) Carbon Cycle Group. The NOAA/ESRL/GMD aircraft measurements of $CH_4$ are made by routinely collecting air samples using 0.7 L silicate glass flasks on biweekly to monthly aircraft flights at over twenty sites. A list of these sites is provided by *Xiong et al.* [2008a]. Air samples are collected using a turboprop aircraft with maximum altitude limits of 300–350 hPa. Twelve to twenty flasks are held in a suitcase-sized container, and collection of air in a single flask at a unique altitude allows a sampling vertical resolution of up to 400 m in the boundary layer. After each flight the flask packages are shipped to the NOAA laboratory in Boulder, Colorado, for trace gas analysis. $CH_4$ samples are measured by gas chromatography (GC) with flame ionization detection (±1.2 ppb) [*Dlugokencky et al.*, 1994]. The individual flights required about 1.5 h to complete. The vertical resolution of 400 m in aircraft measurements is much finer than the vertical resolution of AIRS, so an average of aircraft measurements in several layers will be compared with AIRS retrievals. An average of the AIRS retrievals in a large area over Alaska-Canada or Siberia, as will be defined in section 3.1, is compared with the aircraft measurements. Averaging over these large areas is to minimize random error in the NOAA 3° × 3° gridded products.

[12] Over Surgut, Siberia, aircraft sampling was conducted by the Central Aerological Observatory, Russia. A charter AN-24 aircraft was used with the samples taken by pressurizing air, fed into the cockpit through a drain pipe, into a 0.5 L Pyrex flask using a diaphragm pump. These systems were operated manually with the aircraft sampling at eight different altitudes between 0.5 and 7.0 km, and samples were analyzed in the laboratory of Tohoku University, Japan, and National Institute for Environmental Studies (NIES), Japan [*Machida et al.*, 2001; *Barkley et al.*, 2007]. The $CH_4$ mixing ratios were derived from the flask samples to an accuracy of about 5 ppb, against standard gases, using gas chromatography (GC) equipped with flame ionization detectors. The results are reported in the NIES standard scale [*Tohjima et al.*, 2002].

[13] Since the in situ aircraft measurements over Poker Flat, Alaska, and Surgut, Siberia, were usually carried out below 300 or 350 hPa, and cover most of the altitude range represented by AIRS MUT-$CH_4$, they can be compared to the AIRS MUT-$CH_4$ directly.

### 2.3. Model Simulations

[14] Model simulations are made by the Center for Climate System Research/National Institute for Environmental Studies/Frontier Research Center for Global Change (CCSR/NIES/FRCGC) using an Atmospheric General Circulation Model (AGCM)-based chemistry transport model (hereinafter ACTM). The model simulates atmospheric $CH_4$ at hourly time intervals at a horizontal resolution of T42 spectral truncations (~2.8° × 2.8°) and 67 sigma-pressure vertical layers as described by *Patra et al.* [2009a]. The ACTM meteorology is nudged to horizontal winds and temperature at a Newtonian relaxation time of 1 and 2 days, respectively, from the NCEP DOE/AMIP II reanalysis at 6 h intervals [*Kanamitsu et al.*, 2002] to produce realistic representation of synoptic systems in the AGCM. The trends of methyl chloroform ($CH_3CCl_3$) have been successfully reproduced for the period 1990–2000 using available surface emission inventory (average global totals from *McCulloch and Midgley* [2001]) to constrain the OH in the model [*Patra et al.*, 2009a], and ACTM transport was validated for interhemispheric transport (model and measurement based estimations agree within 10%) using simulation of a dynamical tracer ($SF_6$) with no chemical loss reaction in troposphere [*Patra et al.*, 2009b]. The model simulation is initialized on 1 January 1988 using surface fluxes which are constructed on basis of (1) annual mean anthropogenic/industrial flux distributions from the Emission Database for Global Atmospheric Research (EDGAR, version 3.2) inventory, and (2) the monthly mean natural/biogenic flux distributions from the Goddard Institute for Space Studies (GISS) [*Fung et al.*, 1991]. The EDGAR emissions are provided annually to the model, and interpolated to the model time steps. The GISS wetlands (swamps and bogs), rice cultivation and biomass burning are given a seasonal cycle, and the same seasonal cycle repeats every year (no interannual variability). Interannual variability and trends are considered for the 1988–2000 period in anthropogenic emissions only. Total emissions are held constant after the year 2000. This will contribute to the discrepancy between the model simulations and the AIRS measurements in the seasonal cycle of atmospheric $CH_4$ in our interested period of 2004–2005. For comparison with AIRS retrievals, the model data are sampled at 0130 and 1330 local time each day to match the AIRS overpass time.

[15] Surface emissions of $CH_4$ during the 1990s are computed from a Terrestrial Ecosystem Model (TEM) [*Zhuang et al.*, 2004] for northern wetlands in both Alaska-Canada and Siberia. These data are used for comparison with the $CH_4$ seasonal cycle near the Earth's surface.

### 2.4. Ground-Based Measurements

[16] Data from in situ measurements of $CH_4$ mixing ratio in the MBL in Barrow, Alaska, are obtained from ftp://ftp.cmdl.noaa.gov/ccg/ch4/in-situ/brw [*GLOBALVIEW-CH4*, 2009]. The surface data from many sites are generally used to constrain the chemical transport model in the top-down estimates to infer strengths of sources and sinks [e.g., *Wang et al.*, 2004]. In this work the data from Barrow will be compared with the ACTM simulated data.

### 2.5. Application of Averaging Kernels

[17] To properly compare the satellite observations with model simulations, the model data should be convolved using the averaging kernels and the first guess as below [*Rodgers*, 2000],

$$\hat{x} \approx Ax + (I - A)x_a, \tag{1}$$

where $\hat{x}$ is the convolved model $CH_4$ mixing ratio profile, and $x$ is the profile from the transport model. $x_a$ is the first-guess profile ("a priori"). $I$ is the identity matrix, and $A$ is the averaging kernel matrix. In real application for AIRS, $log(x)$, $log(x_a)$, and $log(\hat{x})$ are used in equation (1) [*Maddy and Barnet*, 2008]. The ACTM data are convolved using the AIRS averaging kernels for the same day and time. In this approach, the difference between AIRS retrievals and the convolved model data will reflect the offset between satellite

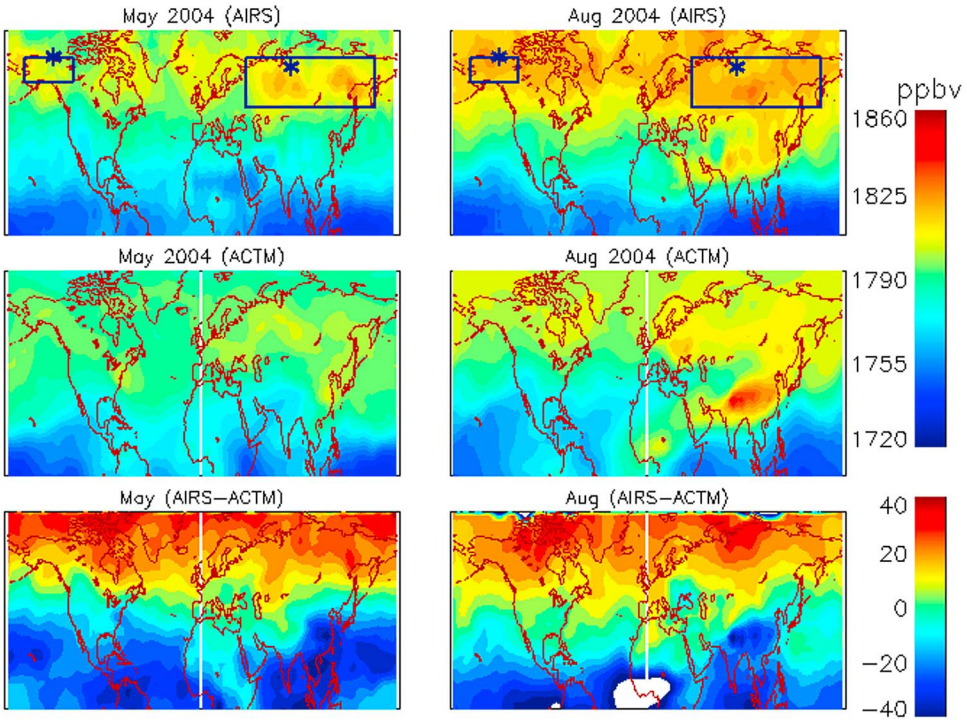


**Figure 1.** Monthly mean distributions of (top) AIRS retrieved and (middle) model-simulated $CH_4$ at 300 hPa for 2 months, (left) May and (right) August. The boxes mark the region of Alaska-Canada (60°N–70°N, 165°W–120°W) and Siberia (50°N–70°N, 40°E–160°E), and asterisks mark the location of aircraft measurements at Poker Flat, Alaska (PFA, 65.07°N, 147.29°W), and Surgut, Siberia (61°N, 73°E). (bottom) The absolute values of the AIRS data minus the model simulations.

observations and the model simulations (as a reference) after taking into account the retrieval smoothing associated with the variation of information content in satellite observations. In section 3.4 we will compare AIRS retrievals with the convolved model data over Alaska-Canada and Siberia.

## 3. Results and Discussion

### 3.1. Spatial Distribution of Mid-Upper Tropospheric $CH_4$ in the HNH

[18] Atmospheric $CH_4$ has a chemical lifetime of about one year near the Earth's surface, and it increases up to about 12 years in the MUT region of the summer hemisphere and more than 1000 years in the winter polar region [*Patra et al.*, 2009b]. Therefore the surface fluxes and atmospheric transport, both having weekly to monthly time scales of variability, mainly control the seasonal variability in the MUT region. In contrast, the chemical loss of $CH_4$ is of equal importance as surface emissions and atmospheric transport near the Earth's surface. The minimum of both observed and model-simulated $CH_4$ concentration is found in the summer near the Earth's surface due to chemical loss [e.g., *Dlugokencky et al.*, 1995; *Patra et al.*, 2009b].

[19] Since wetland emission is one of the most important emission sources in the HNH and has its maximum in summer, we first compare the distribution of mid-upper tropospheric $CH_4$ in the end of spring (May) and in the end of summer (August). As an example, Figure 1 shows the monthly mean distribution of AIRS retrieved $CH_4$ at 300 hPa in May and August in 2004 and its comparison with model simulations. Significant enhancement of $CH_4$ by about 20–30 ppbv in the HNH, particularly over Alaska-Canada and Siberia, is found from May to August. Similar enhancement of AIRS $CH_4$ in a thick layer between 200 and 300 hPa over North America and Eurasia has been discussed by *Xiong et al.* [2008b]. From Figure 1 we can also see the plume of $CH_4$ over south Asia, which is associated with rice paddy emission and the deep convective transport during the summer monsoon season [*Xiong et al.*, 2009a]. For later study on the seasonal variation of $CH_4$ in the HNH, we chose two regions where the wetlands and permafrost regions are mostly located; one is Alaska-Canada (60°N–70°N, 165°W–120°W), and the other is Siberia (50°N–70°N, 40°E–160°E), as marked by the boxes in Figure 1.

[20] Similar to AIRS retrievals, the model simulations (Figure 1, middle) also show the increase of mid-upper tropospheric $CH_4$ from May to August over Alaska-Canada and Siberia. Such an increase in summer is nearly opposite in phase to the seasonality of $CH_4$ concentrations near the Earth's surface, which has higher values in winter and the minimum in summer, as illustrated from many in situ observations [e.g., *Dlugokencky et al.*, 1995]. However, the model-simulated $CH_4$ mixing ratios at 300 hPa are lower than AIRS retrievals in the high-latitude regions and higher near the tropics (see Figure 1, bottom). Part of reason for the lower offset of AIRS retrievals relative to the model results near the tropics is likely associated with the 2% empirical bias correction in absorption coefficients in the AIRS version 5 [*Xiong et al.*, 2008a]. The magnitude of the increase from May to August for AIRS $CH_4$ is similar to the model

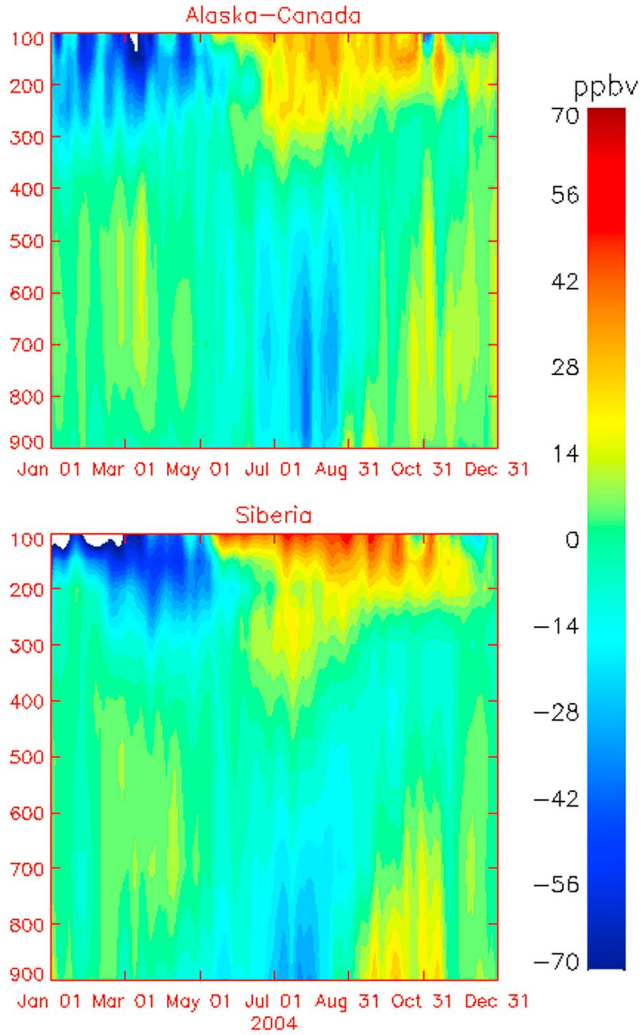


**Figure 2.** Time-pressure cross section of the anomaly of $CH_4$ in (top) Alaska-Canada and (bottom) Siberia, whose areas are as marked in the boxes of Figure 1. Data are from the ACTM simulations in 2004, and the mean in each model level has been removed separately.

simulations over Siberia (the areal averages for both of them are 9 ppbv), but over Alaska-Canada the magnitude of the increase for AIRS $CH_4$ (15 ppbv) is larger than the model simulations (6 ppbv). This larger increase for the AIRS observations over Alaska-Canada may be related to the Alaska forest fire in 2004 [*de Gouw et al.*, 2006; *Duck et al.*, 2007], as this event has not been taken into account in the model simulations. We also note that both AIRS retrievals and model simulations have a small region with high $CH_4$ over Siberia, which may be associated with the strong wetlands emissions in west Siberia, and, for example, has ever been observed from measurements along the Trans-Siberia railroad [*Oberlander et al.*, 2002]. Note that this comparison in Figure 1 is just a rough comparison to illustrate the spatiotemporal difference of the mid-upper tropospheric $CH_4$ between May and August and between the AIRS retrievals and the model simulations. A detail comparison between the model simulations and the AIRS retrievals will be discussed in section 3.4.

### 3.2. Summer Increase of $CH_4$ in the Mid-Upper Troposphere

[21] Model simulations from the ACTM show the $CH_4$ seasonal cycles at different altitudes in the HNH are different, as illustrated from the time-pressure cross section of the $CH_4$ anomaly that is derived from the ACTM simulated results over Alaska-Canada and Siberia (Figure 2). From Figure 2 it is clear that the mid-upper tropospheric $CH_4$ has a significant increase during the summer, and their seasonal cycles are almost opposite to the seasonal cycles of $CH_4$ in the lower troposphere in these two regions. From spring to summer, the mixing ratio of $CH_4$ at 200 hPa increases by 40–50 ppbv, while at 900 hPa it decreases by 20–30 ppbv. The $CH_4$ mixing ratio at 200–300 hPa starts to increase in May–June and stays high in July–August, while the $CH_4$ mixing ratio in the lower troposphere reaches the minimum in July–August.

[22] Since the sampling interval of aircraft measurements of $CH_4$ over PFA and Surgut, Siberia (about 1 or 2 times per month) is sparse compared to the AIRS observations or model simulations, it is hard for these aircraft measurements to capture the summer increase of $CH_4$ in the mid-upper troposphere. However, during the period from late spring to late summer the highest $CH_4$ mixing ratio was usually observed in late June or early July, which provides partial evidence for the summer increase of mid-upper tropospheric $CH_4$. For example, over PFA the largest $CH_4$ mixing ratio at 400–500 hPa in the period from May to August in 2004 and 2005 was observed on 10 July 2004 and 29 June 2005, respectively. To derive the climatology of $CH_4$ in different seasons, we compute the mean profile from aircraft measurements over multiple years, omitting data in the summer of 2003 during which there was a strong forest fire in Siberia. From the mean profile of aircraft measurements over PFA (using data from 1999 to 2006 (Figure 3, top left)) we can see that the $CH_4$ mixing ratio above 600 hPa in summer (June, July and August) has little vertical variation or even increases slightly with altitude, while in other seasons (spring, fall and winter) it decreases with altitude significantly. As the mean profiles for spring, fall and winter decrease with altitude in a similar pattern, for simplicity the $CH_4$ mixing ratios for each level are averaged among these seasons (other than summer) to derive its mean profile. Obviously, in summer the mean $CH_4$ mixing ratio in the lower troposphere is much smaller than in other seasons, but in the middle troposphere the mean $CH_4$ mixing ratio near 400 hPa in summer is close to or even larger than in other seasons. Similarly, the mean profile of aircraft measurements over Surgut (using data from 2003 to 2006 (Figure 3, top right)) shows that in summer $CH_4$ mixing ratio decreases with altitude, especially in the lower troposphere below 600 hPa, but the mean $CH_4$ mixing ratio at 7 km (near 400 hPa) in summer is larger than the mean in other seasons. This difference in $CH_4$ vertical structure between summer and other seasons suggests that the vertical transport of $CH_4$ from the lower to upper troposphere is more efficient in summer.

[23] From Figure 3 we also notice the large difference in summer $CH_4$ in these two regions, for example, over Surgut the $CH_4$ mixing ratio at about 900 hPa is 80 ppbv larger than over Poker Flat, and the vertical decrease of $CH_4$ from 900 hPa to 700 hPa is about 70 ppbv over Surgut as compared

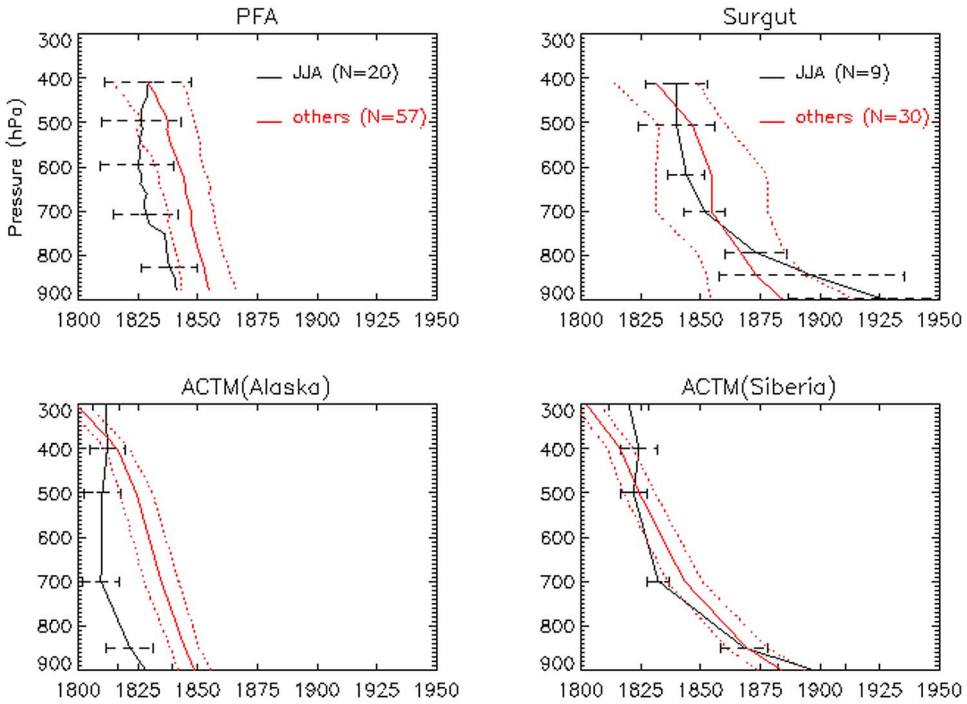


**Figure 3.** (top) Mean profiles and their standard deviations (dashed lines) of aircraft measurements for summer (JJA) and other seasons for regions Poker Flat, Alaska (PFA, 65.07°N, 147.29°W), and Surgut, Siberia (61°N, 73°E). (bottom) The corresponding mean profiles from model simulations averaged in 3 × 3 grid points over Poker Flat, Alaska, and Surgut, Siberia.

to the decrease of about 15 ppbv over PFA. Such a large difference between these two regions is in consistent with the larger regional scale wetland emission around Surgut than around PFA in summer [e.g., *Zhuang et al.*, 2004].

[24] For comparison, the vertical variation of the model-simulated $CH_4$ in each of these two regions, averaged using 9 grid points (3 × 3) over these two sites, is plotted in Figure 3 (bottom). In agreement with in situ aircraft measurements, the model simulations also show the summer increase of $CH_4$ in the mid-upper troposphere along with the smaller summer vertical gradient (as compared to other seasons in both regions). However, the ACTM simulations are biased low by 10–20 ppbv at altitudes above 800 hPa in summertime relative to the in situ measurements.

### 3.3. Seasonal Variation of MUT-$CH_4$ From AIRS and Comparison With Aircraft Measurements and Model Simulations

[25] Figures 4 and 5 show seasonal variations of the AIRS MUT-$CH_4$ over PFA and Surgut, as well as the comparisons with the aircraft measurements and model simulations without using the averaging kernels. Since the AIRS MUT-$CH_4$ represents the mean mixing ratios at a thick layer mostly between ~300–500 hPa (the average tropopause over PFA and Surgut is at ~250 hPa in summer), and the aircraft measurements over PFA are mostly below 300 or 350 hPa, the highest level of aircraft sampling is sometimes below the top level of MUT-$CH_4$. In such situations, only the available aircraft measurements within 500–300 hPa are averaged for comparison. Model results at 300 and 500 hPa are plotted separately in order to illustrate which level is better represented by AIRS MUT-$CH_4$. Due to the large daily variation for AIRS MUT-$CH_4$, we take a biweekly running mean. From Figure 4 we can see that over PFA the AIRS MUT-$CH_4$ increases from late May to mid-July by about 30 ppbv in 2004, then has little increase, or even decrease, from July to mid-August, followed by an increase of about 20 ppbv in late August–early September. The absolute $CH_4$ concentrations and the seasonal cycle at 500 hPa from the model simulations are close to the AIRS retrievals and the aircraft measurements, except in June–July, when the model-simulated $CH_4$ mixing ratios at 300 hPa and 500 hPa are very close, and the phase of $CH_4$ at 300 hPa shows a similar increase as the AIRS retrievals. This result is physically reasonable given the increase of tropopause height in summer, which places the AIRS MUT-$CH_4$ at a higher altitude. Overall, the aircraft measurements capture the seasonal cycle of MUT-$CH_4$, particularly the peak of $CH_4$ in late June to early July in both 2004 and 2005. The largest difference between the aircraft observations and the AIRS MUT-$CH_4$ occurs in September–October in 2004, in which the AIRS MUT-$CH_4$ shows higher concentrations than the aircraft measurements. However, only a few aircraft measurements available in this period from September–October make this comparison difficult. The existence of some difference between aircraft measurements and AIRS observations is understandable since aircraft measurements were taken along a flight track and may not completely represent the large area observed from AIRS.

[26] Over Surgut all the aircraft measurements at level 7 km are compared directly with AIRS MUT-$CH_4$ since it is the closest level to the layer of AIRS MUT-$CH_4$. From Figure 5 it can be seen that the AIRS MUT-$CH_4$ increases from early May, which is about 2 weeks earlier than over

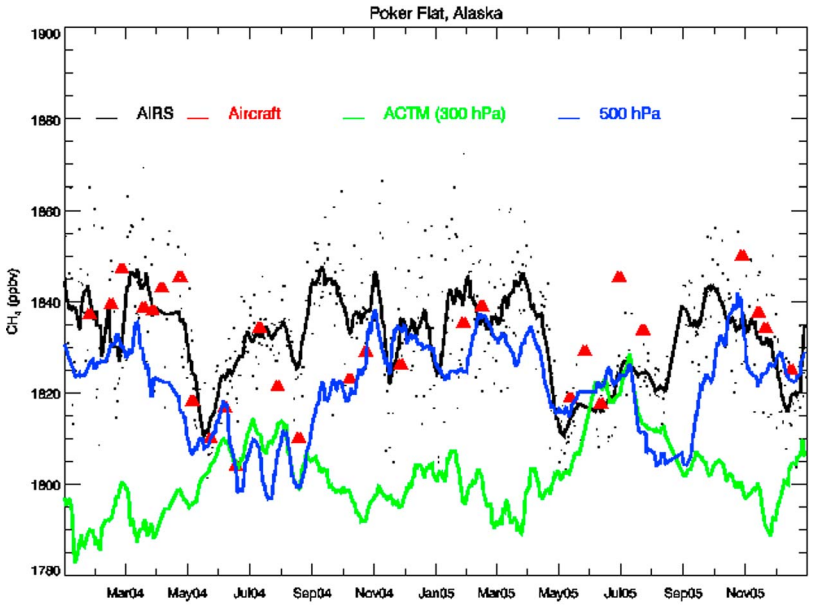


**Figure 4.** Seasonal variation of in situ aircraft measurements over PFA (averaged in layer 50 to 250 hPa below the tropopause) and the AIRS MUT-$CH_4$ over Canada-Alaska. ACTM simulations at 300 and 500 hPa are sampled in the same time and location as the AIRS observations. Black dots are the AIRS retrievals in each day, and the thick black line is its biweekly running mean.

PFA, and there is a slight decrease of about a few ppbv in June followed by an increase until late July. The overall increase from early May to late July is about 25 ppbv. Similar to the observations for PFA, the absolute concentration and seasonal cycle of the model-simulated $CH_4$ at 500 hPa have a better match with AIRS retrievals, and aircraft measurements show a peak in early summer. This early summer peak occurs concurrently with the period when the model-simulated $CH_4$ mixing ratios between 300 hPa and 500 hPa are close to each other. These results again support the notion that the vertical transport of $CH_4$ from the surface to the upper troposphere varies seasonally, and the upward transport of $CH_4$ enriched air from the surface is more efficient in summer compared to other seasons.

### 3.4. Comparison of the Mid-Upper Tropospheric $CH_4$ From AIRS With Model Simulations Using the Averaging Kernels

[27] A detail comparison between the AIRS observations with the model simulations that utilize the AIRS averaging

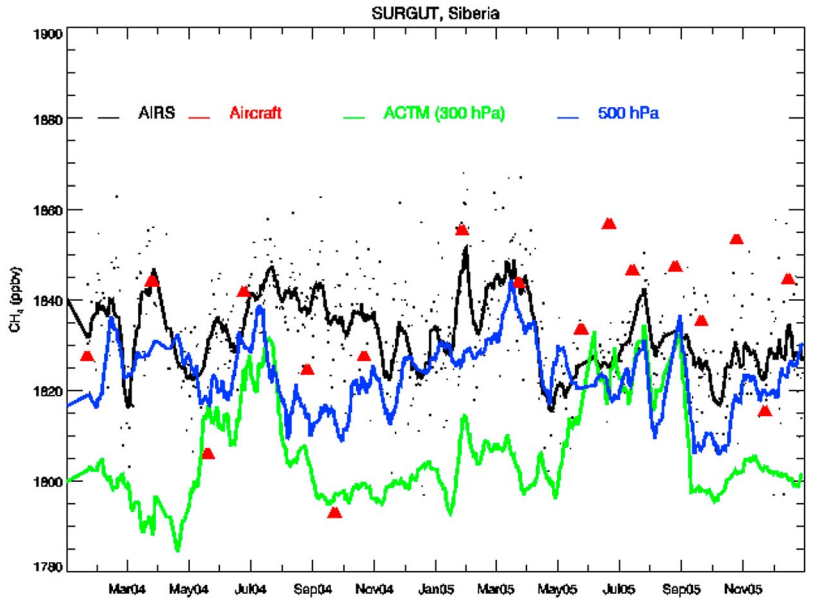


**Figure 5.** Same as Figure 4 but over Surgut, Siberia. An offset of 30 hPa has been removed for model simulations at 900 hPa.

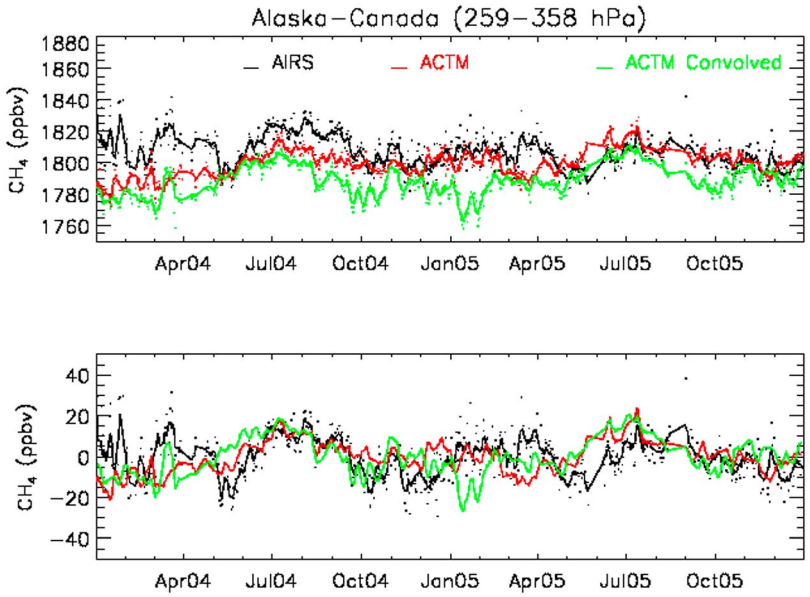


**Figure 6.** (top) The seasonal variation of mid-upper tropospheric $CH_4$ at layer 259–358 hPa from AIRS and its comparison with the ACTM model simulations. Red line is the raw model data and green line is the model simulations convolved using averaging kernels. Black dots are the AIRS retrievals in each day, and thick black line is the running mean over a biweekly window. (bottom) Their anomalies from annual mean.

kernels to convolve the model data is discussed in this section. Figures 6 and 7 show the variation of $CH_4$ for the layer 259–358 hPa, averaged over Alaska-Canada and Siberia, from AIRS and model simulations (convolved) in 2004 and 2005, respectively. For comparison, the raw (not convolved) model-simulated $CH_4$ mixing ratios in this layer are also plotted. The aircraft measurements are not used in this comparison as they are mostly below 300 or 350 hPa. The seasonal cycles can be viewed from the $CH_4$ anomalies, derived by removing the annual mean for each year in 2004 and 2005 (Figures 6 (bottom) and 7 (bottom)).

[28] From Figures 6 and 7 we note a large variation of AIRS $CH_4$, and the variation during summer is smaller than in winter. Due to the large daily variation, a biweekly running mean is applied (the thick lines), from which we can see the magnitudes of the early summer increase (from mid-May to early August) are about 20–30 ppbv over both Alaska-Canada and Siberia. Overall, the seasonal cycle of AIRS retrieved mid-upper tropospheric $CH_4$ has a good agreement with the model simulations in the summer peak. The correlation coefficients between the AIRS retrievals and the model results (convolved) are 0.15 and 0.43 in Alaska-

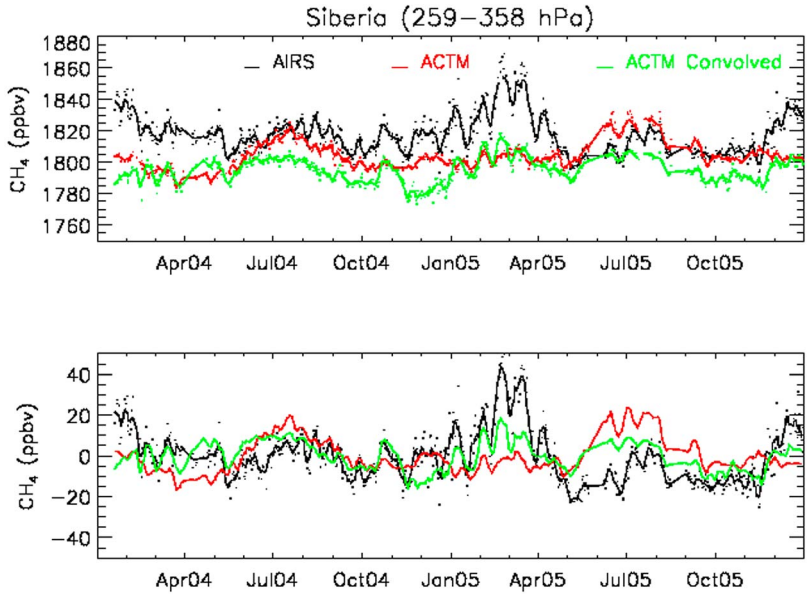


**Figure 7.** Same as Figure 6 but over Siberia.

Canada and Siberia, respectively. If considering only the summer–fall (June–November) data, the correlation coefficients are improved: 0.60 (2004) and 0.27 (2005) for Alaska-Canada, and 0.50 (both in 2004 and 2005) for Siberia. While there is notably less agreement in the 2005 Alaska-Canada case, this may be partially attributed to the missing of data during 17–31 August 2005. This left a small peak for the AIRS retrievals from August to early September 2005, where the model results show a slightly decreasing trend (see Figure 6, bottom). Comparing to the seasonal variation of model results, which has only one peak in summer, AIRS $CH_4$ has another peak in late winter–spring, and in Siberia the maximum of the AIRS retrievals occurs in spring. From Figure 7 (bottom) we can see the maximum in February to March 2005 is obviously artificial as the convolved model data (green line) is significantly higher than the raw model data (red line). We also noted that over Alaska-Canada (Figure 7) the summer $CH_4$ in 2004 is higher than in 2005 by 11 ppbv (averaged in JJA), and this difference may be attributed to the Alaska forest fire in late June to July 2004.

[29] Overall, the model-simulated results are lower than AIRS retrievals. On average, the model results (convolved) are lower than AIRS retrievals −18 ± 13 ppbv in Alaska-Canada, and −23 ± 12 ppbv in Siberia. The largest difference between the AIRS retrievals and model simulations occurs in later winter to early spring, when the AIRS retrievals have a peak. Even removing the annual mean offset between the model simulations and the AIRS retrievals, the model-simulated $CH_4$ (convolved) during January to March is still smaller than AIRS retrieved $CH_4$ −11 ± 14 ppbv over Alaska-Canada and −11 ± 11 ppbv over Siberia. Disregarding the uncertainties in the AIRS retrievals, this large lower bias for the model data relative to AIRS data in late winter–early spring may indicate a lower emission scenario (or some unidentified emission sources, such as the energy use and/or gas leakage) provided in the model, or some discrepancy in transport that is not well represented in the model in winter. The leakage of natural gas was indeed observed from isotopic observations in the Trans-Siberia expeditions, but it is uncertain whether this was a contributor as this leakage was only observed in the vicinity of Novosibirsk city during the spring expedition [*Tarasova et al.*, 2006].

[30] Since the AIRS retrieved $CH_4$ in a layer is not independent [*Xiong et al.*, 2008a], for example, the AIRS retrieved $CH_4$ for the layer 259–358 hPa is a weighted average of $CH_4$ with a greater weight confined to the 259–358 hPa layer and smaller but nonzero weights in its upper and lower layers, to rely solely on the AIRS retrieved $CH_4$ in one layer to interpret the spatiotemporal variation in reality may lead to misleading conclusions in the HNH. This is because the variation of information content of AIRS, which is relatively low in the winter–spring season, and the weighting functions have a large variation. If we assume that the model-simulated $CH_4$ profile is very close to the actual profile in the atmosphere, the discrepancy between the model-simulated raw $CH_4$ data and the convolved data (using equation (1)) can be attributed to the information content change (i.e., the averaging kernels) in the AIRS retrievals, so it can be used as an estimate of the retrieval uncertainty (or retrieval artifact). Statistically, this mean difference between the convolved model data relative to the raw model data in two years from 2004 to 2005 is −9.6 ± 9.5 ppbv (−0.53 ± 0.53%) and −8.1 ± 9.3 ppbv (−0.45 ± 0.52%) in Alaska-Canada and Siberia, respectively, and the corresponding RMS difference is 0.75% and 0.68%. From this estimate the artificial change of AIRS $CH_4$ resulting from the change of information content is roughly less than 0.8%, which is smaller than the AIRS observed summer increase of 20–30 ppbv (about 1.1~1.7%).

## 4. Discussion

[31] The factors influencing the early summer $CH_4$ increase in the mid-upper troposphere include (but not limited to): (1) biomass burning, (2) local emissions, such as emission from northern wetlands, gas leakage or use of energy, and (3) transport, such as the meridional and zonal advection, convection from lower troposphere, or stratosphere-troposphere exchange. We first have a closer look at the seasonal variation of $CH_4$ in the MBL in Barrow, Alaska (71.19°N, 156.36°W) (Figure 8, top) from the in situ observations of the hourly mean mixing ratio in 2004 and 2005, and its comparison with the ACTM simulated $CH_4$ mixing ratios using the data in the closest grid point to Barrow (i.e., 71.16°N and 156.36°W). One interesting feature from the in situ measurements is the frequent occurrence of $CH_4$ spikes, in which the hourly mean is higher than the baseline by at least 20 ppbv, in the period from late June to early November, with the largest spikes mostly occurring in the middle of August. Disregarding the spikes, the seasonal minimum of $CH_4$ in the MBL occurs in July–August and the maximum in January–February. The seasonal cycle of $CH_4$ from the model simulations is overall in a good agreement with in situ observations, however, the model simulations apparently miss the spikes, which is partly due to its coarse horizontal resolution (300 × 300 km) not being adequate for a coastal site like Barrow (and a region around point sources). In addition, the model simulations are biased low relative to the in situ measurements during later winter to spring, and the annual mean of the model-simulated $CH_4$ mixing ratio is less than the in situ observations by 27 and 13 ppbv in 2004 and 2005, respectively.

[32] A comparison of $CH_4$ in the MBL in Alaska between 2004 and 2005 indicates that the in situ measurements in 2004 are apparently higher and have more spikes than in 2005 (Figure 8). On average from 15 June to 15 November, the mean $CH_4$ mixing ratio in 2004 is ~25 ppbv higher than in 2005, and ~15 ppbv higher than in 2003 and 2006 (not shown). Moreover, the number of spikes, if defined as the data points with their hourly mean mixing ratios above 1900 ppbv, is about 23% and 12% of all measurements for 2004 and 2005, respectively. The higher $CH_4$ mixing ratios as well as more spikes in the summertime of 2004 are probably related to the 2004 Alaska forest fire.

[33] Both the ground-based measurements and the model simulations at Barrow, Alaska, show a decrease of $CH_4$ in the MBL in late spring (March–May), and the reason is the breakdown of the atmospheric inversion layers, which allows dilution of $CH_4$ in the lower troposphere by mixing with the air from the middle and upper troposphere at northern high latitudes [*Kahl*, 1990; *Dlugokencky et al.*, 1995]. The impact of stratosphere-troposphere exchange

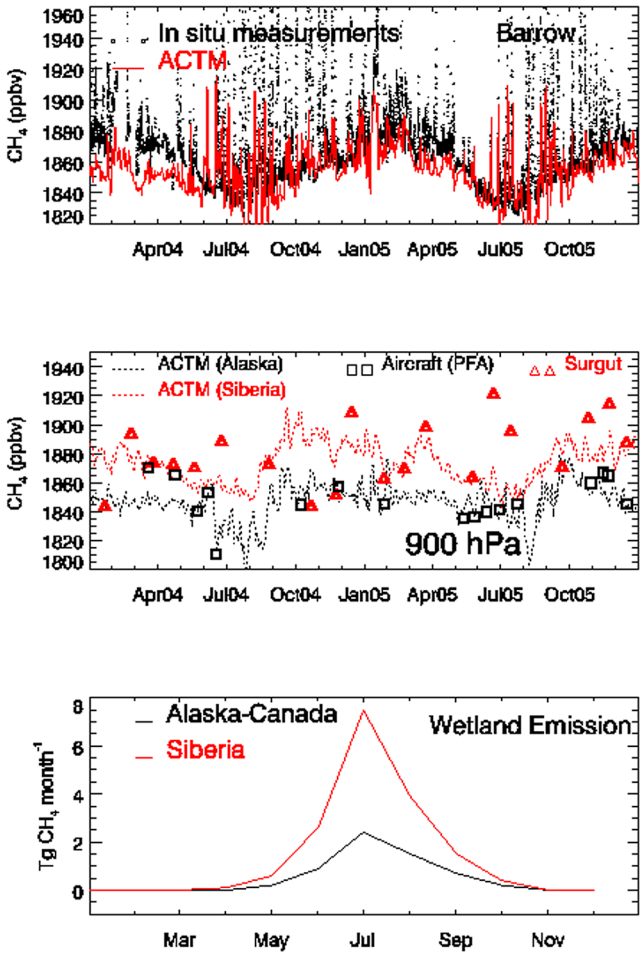


**Figure 8.** (top) $CH_4$ in the MBL from the ACTM simulations and in situ measurements in Barrow, Alaska, by NOAA/ESRL/GMD. (middle) Comparison of the model-simulated and aircraft-measured $CH_4$ near 900 hPa in two regions. (bottom) The monthly average of model-simulated wetland emission for the 1990s in Alaska-Canada and Siberia [*Zhuang et al.*, 2004].

on the decrease of mid-upper tropospheric $CH_4$ in late spring can also be envisaged, as shown in the case of $N_2O$ using the ACTM simulations and measurements in the upper troposphere and lower stratosphere region [*Ishijima et al.*, 2010]. A brief discussion of the meridional and zonal advection transport will be given next, and our focus is on the impact from the enhanced vertical transport and the wetland emission during summer.

### 4.1. Impact of Enhanced Convection in Summer

[34] Both the aircraft measurements and the ACTM simulations indicate that the $CH_4$ vertical gradient in the middle-upper troposphere in summer is smaller than in other seasons, suggesting the efficient transport of $CH_4$ from the lower to upper troposphere in summer. To examine the impact of transport, Figures 9a and 9b show that latitude-pressure distributions of $CH_4$ from the ACTM simulations overlaid with vertical pressure velocity in February and August, respectively. During the wintertime (i.e., February) there is a weaker vertical transport of surface $CH_4$ to the middle and upper troposphere regions (i.e., closely spaced $CH_4$ isolines) in the HNH, and a weaker transport from the high latitudes to the tropical latitudes (due to the presence of the strong subtropical jet around 25°N). This trapping of air in the troposphere plus the small chemical loss due to OH reaction lead to higher $CH_4$ concentration near the surface in HNH during winter [*Patra et al.*, 2009b]. In contrast, during summer (i.e., August) both the $CH_4$ latitudinal gradient from the HNH toward the tropical latitudes and the vertical gradient from surface toward the upper/middle troposphere are much lower than in winter. This is due to the enhanced vertical mixing that is associated with the increased convective activities in the northern high latitudes (60–90°) during summer (vertical pressure velocity 0–3 hPa $d^{-1}$) relative to the strong downward motion during winter (vertical pressure velocity 3–9 hPa $d^{-1}$), and the shift in intertropical convergence zone (ITCZ; seen as vertical pressure velocity greater than −20 hPa $d^{-1}$) from about 15°S in winter to about 15°N in summer. Note that the summer meteorological condition and the increased chemical loss in NH also lead to weaker interhemispheric gradient in $CH_4$ in the lower troposphere (below 400 hPa).

[35] From the latitude-longitude distributions at 300 hPa and 400 hPa (Figures 9c–9f), we can see the meridional and zonal transport. In wintertime the typical origin of air mass over Alaska is mostly from the Pacific Ocean (convergence), while over Siberia the origin of air mass is mostly from European regions transporting to higher-latitude regions [*Patra et al.*, 2009c]. A higher $CH_4$ over Siberia than over Alaska in winter may be partly related with this transport from Europe. In summertime the meridional advection transport under the impact of prevalent westerly winds is dominant, but the transport northeastward along the north branch of the Tibetan anticyclone may bring some $CH_4$ to Siberia from the $CH_4$ plume over south Asia [*Xiong et al.*, 2009a].

[36] It should be noted that the amplitude of the $CH_4$ seasonal cycle in the mid-upper troposphere is usually much smaller than in the lower troposphere, and the increase of mid-upper tropospheric $CH_4$ in summer does not imply that the absolute $CH_4$ concentrations in the mid-upper troposphere have to be significantly larger than in the lower troposphere. The enhanced vertical transport since early summer leads to better mixing between the lower tropospheric air (with enriched $CH_4$) with the air in the upper levels, and consequently, reduces the vertical gradient of $CH_4$ in summer (see Figure 3). As the $CH_4$ seasonal cycle near the surface is mainly controlled by the balance between the surface emissions and the chemical loss due to OH reaction, and the loss apparently exceeds the increase in emissions from boreal winter to summer in most regions [*Patra et al.*, 2009a], thus resulting in lower mixing ratios in summer compared to winter in the lower troposphere. Even the $CH_4$ mixing ratio in the lower troposphere decreases in summer, its value is, in general, larger than that in the upper troposphere, thus the vertical convection transport leads to the increase of $CH_4$ in the mid-upper troposphere.

### 4.2. Impact of Wetland Emission

[37] From Figure 3 we have found that over Poker Flat the mean $CH_4$ mixing ratio in summer is mostly smaller than in other seasons (except in the mid-upper troposphere), but

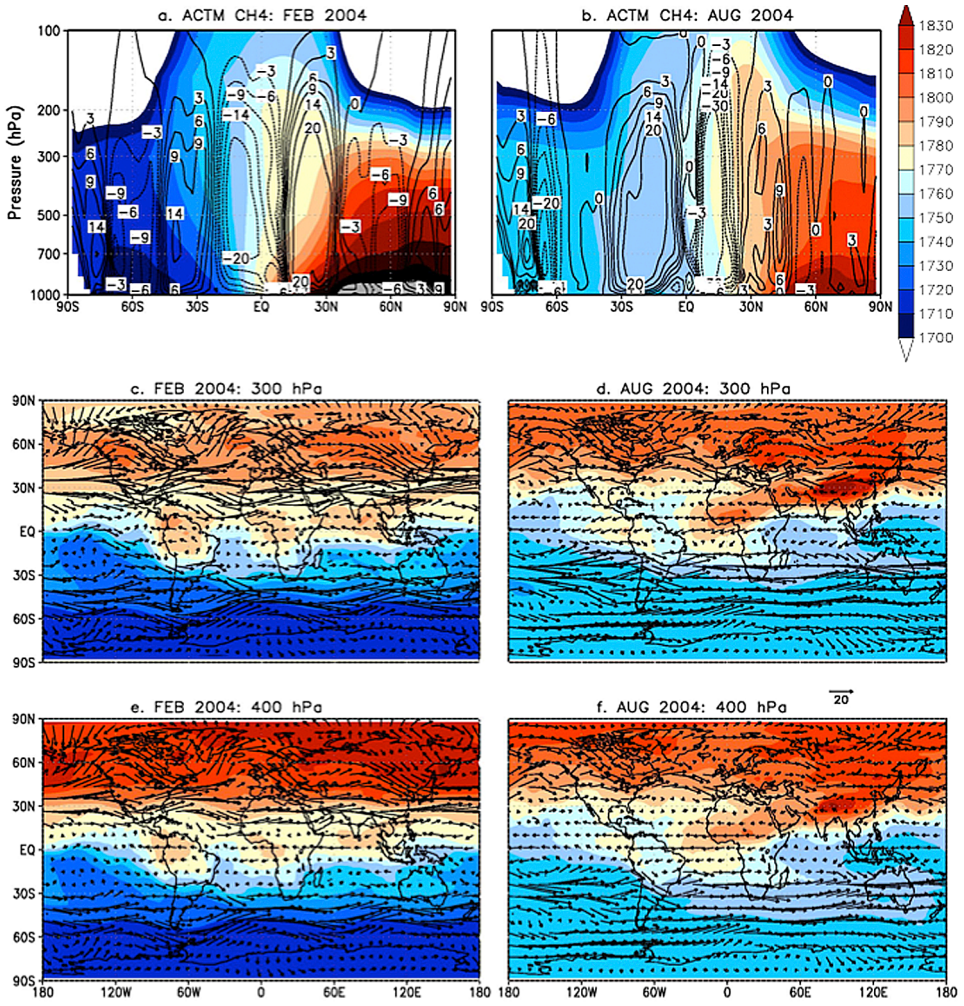


**Figure 9.** (a and b) Zonal mean latitude-pressure distributions, and latitude-longitude distributions at (c and d) 300 hPa and (e and f) 400 hPa of the modeled tropospheric $CH_4$. The vertical pressure velocity (hPa $d^{-1}$; the positive and negative values represent downward and upward motions, respectively) and horizontal wind vectors are shown on Figures 9a and 9b and Figures 9c–9f, respectively.

over Surgut the mean $CH_4$ profile in summer is larger than in other seasons in both the lower troposphere (below 800 hPa) and the mid-upper troposphere (above 450 hPa). This regional difference in the lower troposphere can be better illustrated by observing $CH_4$ near 900 hPa (Figure 8, middle). Due to availability of aircraft sampling, over Surgut the aircraft measurements at level of 1 km are plotted. In agreement with the aircraft measurements, the model-simulated $CH_4$ mixing ratios at 900 hPa over Siberia are overall larger than over Alaska-Canada by about 50 ppbv. In layer 400–600 hPa the $CH_4$ mixing ratio over Surgut is about 10–20 ppbv higher than over PFA (Figure 3). These differences in $CH_4$ between these two regions indicate that there are stronger emission sources over Siberia than over Alaska-Canada, and the local emissions not only have a significant impact on $CH_4$ distribution in the lower troposphere but also in the mid-upper troposphere.

[38] One of the major $CH_4$ sources in west Siberia is from wetlands emission in summertime [*Oberlander et al.*, 2002; *Tarasova et al.*, 2006]. Of all the different emission sources in the high northern latitudes, the wetland emission is the one that has a significant seasonal variation in addition to biomass burning. Alaska-Canada, Western Russia and Siberia are densely covered by wetlands, and they are usually frozen and covered by the snow in winter and early spring. The emission of $CH_4$ from the ground is very low if not zero during these periods, except for possible large $CH_4$ emissions from Arctic tundra during the onset of freezing [*Mastepanov and Christensen*, 2008]. As snow starts to melt in the late spring, the soil temperature starts to increase; in summer the vegetation grows quickly. $CH_4$ emission thus starts to increase in the late spring or early summer. From model simulations by *Zhuang et al.* [2004], the $CH_4$ emissions from northern wetlands in both Alaska-Canada and Siberia significantly increase after June, and the maxima in these two regions occur in July, as illustrated in Figure 8 (bottom). The total emission from Siberia is 2.8 times larger than from Alaska-Canada. Although some leakage of natural gas was observed from isotopic observations from Trans-Siberian railroad [*Tarasova et al.*, 2006], the emissions from wetlands are apparently much larger from this region as it is estimated that annual total emissions of 19.8 Tg-$CH_4$ from Russian gas

production [*Olivier and Berdowski*, 2001] and 33 Tg-$CH_4$ from Siberian wetland emission [*Zhuang et al.*, 2004]. While emissions from gas production are relatively large, we expect these emissions to be more constant throughout the year. In contrast, emissions from wetlands occur mostly in summer, so they are likely to play an important role on the seasonal cycle of $CH_4$ not only in the lower troposphere but also in the mid-upper troposphere.

## 5. Summary and Conclusions

[39] AIRS has allowed spaceborne measurement of global $CH_4$ in mid to upper troposphere from September 2002 to the present. Two years of NOAA AIRS retrieval products in 2004 and 2005 were used to illustrate the spatiotemporal variation of mid-upper tropospheric $CH_4$ in the high Northern Hemisphere (HNH). Aircraft measurements at Poker Flat, Alaska, and Surgut, Siberia, along with model simulations from a forward chemistry-transport model (ACTM), were analyzed correspondingly. Taking into account the variation of the information content of AIRS with time and location, the retrievals at the layer 50 to 250 hPa below the tropopause were used for analysis of the seasonal cycle of $CH_4$ in the mid-upper troposphere (MUT-$CH_4$). The retrieved $CH_4$ were also compared with the model simulations convolved using the AIRS averaging kernels. From these analyses we found the following.

[40] 1. In contrast to the general seasonal cycle of $CH_4$ in the marine boundary layer (MBL) that shows the minimum in the summer, the mid-upper tropospheric $CH_4$ in the HNH increases from May–June through the summer, as evident from both AIRS observations and the ACTM simulations. Although the sampling intervals of in situ aircraft measurements were sparse, the climatology of the profile derived from multiple years' data showed the $CH_4$ vertical gradient during summer season is much smaller than in other seasons, and the mean MUT-$CH_4$ in summer is close to or larger than that in other seasons. In the MBL the ACTM simulated $CH_4$ seasonal cycle has a fairly good agreement with in situ observations in Barrow, Alaska.

[41] 2. From the difference of $CH_4$ between 2004 and 2005 (in both AIRS retrievals in mid-upper troposphere and the spikes of $CH_4$ from ground-based measurements), the 2004 Alaska forest fire apparently leads to some increase of $CH_4$.

[42] 3. Compared to the AIRS retrievals and the in situ aircraft measurements, the ACTM model-simulated $CH_4$ mixing ratios are biased low by about 10–20 ppbv in the mid-upper troposphere. Similarly, the model is biased low in the MBL as compared to ground-based measurements in winter−spring. The model-observation differences in late winter to early spring may suggest some unidentified emission sources, such as the leakage of natural gases, or use of energy, or some deficiency in the model simulations. However, because the observation from space in the polar winter is more challenging and the uncertainties of AIRS retrievals are relatively larger, further improvements to the retrieval algorithm and validation, as well as the use of data from other satellite measurements, such as IASI and TANSO/GOSAT, are necessary to confirm and quantify the existence of unidentified emission sources.

[43] The difference of $CH_4$ seasonal cycles in the mid-upper troposphere from those in the MBL is a unique finding in this study. Further examination of the mechanism controlling the summer increase of $CH_4$ in the mid-upper troposphere will need additional model simulations to quantify the impacts of different factors, which is out of the scope of this paper. However, from our preliminary analysis in this paper we believe that the enhanced convection is likely an important factor because it leads to a smaller vertical gradient of $CH_4$ in summer than in other seasons. The regional difference between Alaska-Canada and Siberia, in terms of the absolute mixing ratios, emissions and the seasonal cycles in different altitudes, suggests the impact of local emissions on the variation of $CH_4$ not only in the lower troposphere but also in the mid-upper troposphere. Future monitoring in high northern latitudes is important for quantifying emissions from northern wetlands.

[44] To our knowledge, this study is the first attempt at synthesizing model results, aircraft measurements and satellite observations to investigate the seasonal cycle of $CH_4$ in the mid-upper troposphere in the HNH. Considering the large difference in spatial resolution and sampling time among these three data sets, some disagreements among them are expected. These analyses are thus limited as (1) the sampling intervals of aircraft measurements are sparse and random, (2) the altitudes sampled by aircraft measurements are mostly lower than the most sensitive layer of AIRS, (3) interannual variation in fluxes was not included in the ACTM simulations, and (4) satellite observations from AIRS are more challenging in the HNH and its validation is still limited. Further validation and improvements on the retrieval algorithm are required and will be an ongoing project with the availability of more recent aircraft measurements, such as ARCTAS.

[45] **Acknowledgments.** This research was supported by funding from NOAA Office of Application and Research. The views, opinions, and findings contained in this paper are those of the authors and should not be construed as an official National Oceanic and Atmospheric Administration or U.S. government position, policy, or decision. This study also benefits from a Methane Working Group supported by the National Center of Ecological Analysis and Synthesis (NCEAS). We thank Central Aerological Observatory, Russia, for conducting Surgut sampling and T. Nakazawa, Tohoku University, for $CH_4$ analysis before 2005. Also, we thank Nicholas R. Nalli from NOAA/NESDIS for his kind help in editing the whole manuscript and providing professional feedback, and we thank three anonymous reviewers for their comments and constructive suggestions.

## References

Aumann, H. H., et al. (2003), AIRS/AMSU/HSB on the Aqua mission: Design, science objectives, data products, and processing systems, *IEEE Trans. Geosci. Remote Sens.*, *41*, 253–264, doi:10.1109/TGRS.2002.808356.

Barkley, M. P., et al. (2007), Assessing the near surface sensitivity of SCIAMACHY atmospheric $CO_2$ retrieved using (FSI) WFM-DOAS, *Atmos. Chem. Phys.*, *7*, 3597–3619, doi:10.5194/acp-7-3597-2007.

Bloom, A. A., P. I. Palmer, A. Fraser, D. S. Reay, and C. Frankenberg (2010), Large-scale controls of methanogenesis inferred from methane and gravity spaceborne data, *Science*, *327*, 322–325, doi:10.1126/science.1175176.

Bousquet, P., et al. (2006), Contribution of anthropogenic and natural sources to atmospheric methane variability, *Nature*, *443*, 439–443, doi:10.1038/nature05132.

Brasseur, G. P., J. Orlando, and G. Tyndall (Eds.) (1999), *Atmospheric Chemistry and Global Change*, Oxford Univ. Press, New York.

Butler, T. M., P. J. Rayner, I. Simmonds, and M. G. Lawrence (2005), Simultaneous mass balance inverse modeling of methane and carbon monoxide, *J. Geophys. Res.*, *110*, D21310, doi:10.1029/2005JD006071.

Christensen, T. R., T. Johanson, H. J. Akerman, and M. Mastepanov (2004), Thawing sub-arctic permafrost: Effects on vegetation and methane emissions, *Geophys. Res. Lett.*, *31*, L04501, doi:10.1029/2003GL018680.

Clerbaux, C., J. Hadji-Lazaro, S. Turquety, G. Mégie, and P.-F. Coheur (2003), Trace gas measurements from infrared satellite for chemistry and climate applications, *Atmos. Chem. Phys.*, *3*, 1495–1508, doi:10.5194/acp-3-1495-2003.

Crevoisier, C., D. Nobileau, A. M. Fiore, R. Armante, A. Chédin, and N. A. Scott (2009), A new insight on tropospheric methane in the Tropics—First year from IASI hyperspectral infrared observations, *Atmos. Chem. Phys. Discuss.*, *9*, 6855–6887, doi:10.5194/acpd-9-6855-2009.

de Gouw, J. A., et al. (2006), Volatile organic compounds composition of merged and aged forest fire plumes from Alaska and western Canada, *J. Geophys. Res.*, *111*, D10303, doi:10.1029/2005JD006175.

Dlugokencky, E. J., L. P. Steele, P. M. Lang, and K. A. Masarie (1994), The growth rate and distribution of atmospheric methane, *J. Geophys. Res.*, *99*, 17,021–17,043, doi:10.1029/94JD01245.

Dlugokencky, E. J., L. P. Steele, P. M. Lang, and K. A. Masarie (1995), Atmospheric methane at Mauna Loa and Barrow observatories: Presentation and analysis of it situ measurements, *J. Geophys. Res.*, *100*, 23,103–23,113, doi:10.1029/95JD02460.

Dlugokencky, E. J., B. P. Walter, K. A. Masarie, P. M. Lang, and E. S. Kasischke (2001), Measurement of an anomalous global methane increase during 1998, *Geophys. Res. Lett.*, *28*, 499–502, doi:10.1029/2000GL012119.

Dlugokencky, E. J., S. Houweling, L. Bruhwiler, K. A. Masarie, P. M. Lang, J. B. Miller, and P. P. Tans (2003), Atmospheric methane levels off: Temporary pause or a new steady-state?, *Geophys. Res. Lett.*, *30*(19), 1992, doi:10.1029/2003GL018126.

Dlugokencky, E. J., et al. (2009), Observational constraints on recent increases in the atmospheric $CH_4$ burden, *Geophys. Res. Lett.*, *36*, L18803, doi:10.1029/2009GL039780.

Duck, T. J., et al. (2007), Transport of forest fire emissions from Alaska and the Yukon Territory to Nova Scotia during summer 2004, *J. Geophys. Res.*, *112*, D10S44, doi:10.1029/2006JD007716.

Fiore, A. M., L. W. Horowitz, E. J. Dlugokencky, and J. J. West (2006), Impact of meteorology and emissions on methane trends, 1990–2004, *Geophys. Res. Lett.*, *33*, L12809, doi:10.1029/2006GL026199.

Frankenberg, C., P. Bergamaschi, A. Butz, S. Houweling, J. F. Meirink, J. Notholt, A. K. Petersen, H. Schrijver, T. Warneke, and I. Aben (2008), Tropical methane emissions: A revised view from SCIAMACHY onboard ENVISAT, *Geophys. Res. Lett.*, *35*, L15811, doi:10.1029/2008GL034300.

Fung, I., J. John, J. Lerner, E. Matthews, M. Prather, L. P. Steele, and P. J. Fraser (1991), Three-dimensional model synthesis of the global methane cycle, *J. Geophys. Res.*, *96*, 13,033–13,065, doi:10.1029/91JD01247.

GLOBALVIEW-CH4 (2009), *Cooperative Atmospheric Data Integration Project—Methane* [CD-ROM], ESRL, NOAA, Boulder, Colo.

Heimann, M. (2010), How stable is the methane cycle?, *Science*, *327*, 1211–1212, doi:10.1126/science.1187270.

Houweling, S., F. Dentener, J. Lelieveld, B. Walter, and E. Dlugokencky (2000), The modeling of tropospheric methane: How well can point measurements be reproduced by a global model?, *J. Geophys. Res.*, *105*, 8981–9002, doi:10.1029/1999JD901149.

Intergovernmental Panel on Climate Change (2007), *Climate Change 2007: The Physical Science Basis*, edited by S. Solomon et al., Cambridge Univ. Press, Cambridge, U. K.

Ishijima, K., et al. (2010), The stratospheric influence on the seasonal cycle of nitrous oxide in the troposphere deduced from aircraft observations and a model, *J. Geophys. Res.*, doi:10.1029/2009JD013322 in press.

Jacob, D. J., et al. (2010), The ARCTAS aircraft mission: Design and execution, *Atmos. Chem. Phys.*, *10*, 5191–5212, doi:10.5194/acp-10-5191-2010.

Kahl, J. D. (1990), Characteristics of the low-level temperature inversion along the Alaskan Arctic coast, *Int. J. Climatol.*, *10*, 537–548, doi:10.1002/joc.3370100509.

Kanamitsu, M., W. Ebisuzaki, J. Woollen, S. K. Yang, J. J. Hnilo, M. Fiorino, and G. Potter (2002), NCEP-DOE AMIP-II reanalysis, *Bull. Am. Meteorol. Soc.*, *83*, 1631–1643, doi:10.1175/BAMS-83-11-1631(2002)083<1631:NAR>2.3.CO;2.

Machida, T., et al. (2001), Temporal and spatial variations of atmospheric $CO_2$ mixing ratio over Siberia, paper presented at Sixth International $CO_2$ Conference, World Meteorol. Org., Sendai, Japan.

Maddy, E. S., and C. D. Barnet (2008), Vertical resolution estimates in Version 5 of AIRS operational retrievals, *IEEE Trans. Geosci. Remote Sens.*, *46*(8), 2375–1384, doi:10.1109/TGRS.2008.917498.

Mastepanov, M., and T. R. Christensen (2008), Large tundra methane burst during onset of freezing, *Nature*, *456*, 628-630, doi:10.1038/nature07464.

McCulloch, A., and P. M. Midgley (2001), The history of methyl chloroform emissions: 1951–2000, *Atmos. Environ.*, *35*, 5311–5319, doi:10.1016/S1352-2310(01)00306-5.

Nakazawa, T., T. Machida, M. Tanaka, Y. Fujii, S. Aoki, and O. Watanabe (1993), Differences of the atmospheric $CH_4$ concentration between the Arctic and Antarctic regions in pre-industrial/pre-agricultural era, *Geophys. Res. Lett.*, *20*, 943–946, doi:10.1029/93GL00776.

Oberlander, E. A., et al. (2002), Trace gas measurements along the Trans-Siberian railroad: The TROICA 5 expedition, *J. Geophys. Res.*, *107*(D14), 4206, doi:10.1029/2001JD000953.

Olivier, J. G. J., and J. J. M. Berdowski (2001), Global emissions sources and sinks, in *The Climate System*, edited by J. Berdowski, R. Guicherit, and B. J. Heij, pp. 33–78, A.A. Balkema, Lisse, Netherlands.

Patra, P. K., et al. (2009a), Growth rate, seasonal, synoptic, diurnal variations and budget of methane in lower atmosphere, *J. Meteorol. Soc. Jpn.*, *87*(4), 635–663, doi:10.2151/jmsj.87.635.

Patra, P. K., M. Takigawa, G. S. Dutton, K. Uhse, K. Ishijima, B. R. Lintner, K. Miyazaki, and J. W. Elkins (2009b), Transport mechanisms for synoptic, seasonal and interannual SF6 variations and "age" of air in troposphere, *Atmos. Chem. Phys.*, *9*, 1209–1225, doi:10.5194/acp-9-1209-2009.

Patra, P. K., X. Xiong, C. Barnet, E. J. Dlugokencky, U. Karin, K. Tsuboi, and D. Worthy (2009c), Validation of $CH_4$ surface emission using forward chemistry-transport model, paper presented at 18th International Emission Inventory Conference: Comprehensive Inventories—Leveraging Technology and Resources, U.S. Environ. Prot. Agency, Baltimore, Md.

Payette, S., A. Delwaide, M. Caccianiga, and M. Beauchemin (2004), Accelerated thawing of subarctic peatland permafrost over the last 50 years, *Geophys. Res. Lett.*, *31*, L18208, doi:10.1029/2004GL020358.

Payne, V. H., S. A. Clough, M. W. Shephard, R. Nassar, and J. A. Logan (2009), Information-centered representation of retrievals with limited degrees of freedom for signal: Application to methane from the Tropospheric Emission Spectrometer, *J. Geophys. Res.*, *114*, D10307, doi:10.1029/2008JD010155.

Rasmussen, R. A., and M. A. K. Khalil (1984), Atmospheric methane in recent and ancient atmospheres: Concentrations, trends, and interhemispheric gradient, *J. Geophys. Res.*, *89*, 11,599–11,605, doi:10.1029/JD089iD07p11599.

Razavi, A., C. Clerbaux, C. Wespes, L. Clarisse, D. Hurtmans, S. Payan, C. Camy-Peyret, and P. F. Coheur (2009), Characterization of methane retrievals from the IASI space-borne sounder, *Atmos. Chem. Phys. Discuss.*, *9*, 7615–7643, doi:10.5194/acpd-9-7615-2009.

Rigby, M., et al. (2008), Renewed growth of atmospheric methane, *Geophys. Res. Lett.*, *35*, L22805, doi:10.1029/2008GL036037.

Rodgers, C. D. (2000), *Inverse Methods for Atmospheric Sounding*, *World Sci.*, Hackensack, N. J.

Shakhova, N., I. Semiletov, A. Salyuk, V. Yusupov, D. Kosmach, and O. Gustafsson (2010), Extensive methane venting to the atmosphere from sediments of the East Siberia Arctic shelf, *Science*, *327*, 1246–1250, doi:10.1126/science.1182221.

Simpson, I. J., T.-Y. Chen, D. R. Blake, and F. S. Rowland (2002), Implications of the recent fluctuations in the growth rate of tropospheric methane, *Geophys. Res. Lett.*, *29*(10), 1479, doi:10.1029/2001GL014521.

Tarasova, O. A., C. A. M. Brenninkmeijer, S. S. Assonov, N. F. Elansky, and T. Röckmann (2006), Atmospheric CH4 along the Trans-Siberian railroad (TROICA) and river Ob: Source identification using stable isotope analysis, *Atmos. Environ.*, *40*, 5617–5628, doi:10.1016/j.atmosenv.2006.04.065.

Tohjima, Y., T. Machida, M. Utiyama, M. Katsumoto, and Y. Fujinuma (2002), Analysis and presentation of in situ atmospheric methane measurements from Cape Ochi-ishi and Hateruma Island, *J. Geophys. Res.*, *107*(D12), 4148, doi:10.1029/2001JD001003.

Walter, K. M., et al. (2006), Methane bubbling from Siberian thaw lakes as a positive feedback to climate warming, *Nature*, *443*, doi:10.1038/nature05040.

Walter, K. M., et al. (2007), Methane bubbling from northern lakes: Present and future contributions to the global methane budget, *Philos. Trans. R. Soc. A*, *365*, 1657–1676, doi:10.1098/rsta.2007.2036.

Wang, J. S., J. A. Logan, M. B. McElroy, B. N. Duncan, I. A. Megretskaia, and R. M. Yantosca (2004), A 3-D model analysis of the slowdown and interannual variability in the methane growth rate from 1988 to 1997, *Global Biogeochem. Cycles*, *18*, GB3011, doi:10.1029/2003GB002180.

Xiong, X., C. Barnet, E. Maddy, C. Sweeney, X. Liu, L. Zhou, and M. Goldberg (2008a), Characterization and validation of methane

products from the Atmospheric Infrared Sounder (AIRS), *J. Geophys. Res.*, *113*, G00A01, doi:10.1029/2007JG000500.

Xiong, X., C. D. Barnet, E. Maddy, X. Liu, and M. Goldberg (2008b), Variation of atmospheric methane over the permafrost regions from satellite observation during 2003 to 2007, paper presented at Ninth International Conference on Permafrost, Univ. of Alaska Fairbanks, Fairbanks.

Xiong, X., C. Barnet, J. Wei, and E. Maddy (2009a), Information-based mid-upper tropospheric methane derived from Atmospheric Infrared Sounder (AIRS) and its validation, *Atmos. Chem. Phys. Discuss.*, *9*, 16,331–16,360, doi:10.5194/acpd-9-16331-2009.

Xiong, X., S. Houweling, J. Wei, E. Maddy, F. Sun, and C. D. Barnet (2009b), Methane plume over South Asia during the monsoon season: Satellite observation and model simulation, *Atmos. Chem. Phys.*, *9*, 783–794, doi:10.5194/acp-9-783-2009.

Yokota, T., T. Aoki, N. Eguchi, Y. Ota, Y. Yoshida, S. Oshchepkov, A. Bril, R. Desbiens, and I. Morino (2008), Data retrieval algorithms of the SWIR bands of the TANSO-FTS sensor aboard GOSAT, *J. Remote Sens. Soc. Jpn*, *28*(2), 133–142.

Zhuang, Q., J. M. Melillo, D. W. Kicklighter, R. G. Prinn, A. D. McGuire, P. A. Steudler, B. S. Felzer, and S. Hu (2004), Methane fluxes between terrestrial ecosystems and the atmosphere at northern high latitudes during the past century: A retrospective analysis with a process-based biogeochemistry model, *Global Biogeochem. Cycles*, *18*, GB3010, doi:10.1029/2004GB002239.

Zhuang, Q., J. M. Melack, S. Zimov, K. M. Walter, C. L. Butenhoff, and M. A. K. Khalil (2009), Global methane emissions from wetlands, rice paddies, and lakes, *Eos Trans. AGU*, *90*(5), 37–38, doi:10.1029/2009EO050001.

Zimov, S. A., et al. (2006), Climate change: Permafrost and the global carbon budget, *Science*, *312*, 1612–1613, doi:10.1126/science.1128908.

C. D. Barnet and X. Xiong, Center for Satellite Applications and Research, National Environmental Satellite, Data, and Information Service, NOAA, Camp Springs, MD 20746, USA. (xiaozhen.xiong@noaa.gov)

T. Machida, CGER, National Institute for Environmental Studies, Tsukuba, Ibaraki 305-8506, Japan.

P. K. Patra, Research Institute for Global Change, JAMSTEC, Yokohama 236 001, Japan.

C. Sweeney, Global Monitoring Division, ESRL, NOAA, Boulder, CO 80305, USA.

Z. Zhuang, Department of Earth and Atmospheric Sciences, Purdue University, West Lafayette, IN 47906, USA.